Absorption of Siderite Within a Chemically Modified Poly(lactic acid) Based Composite Material for Agricultural Applications

Nancy L. Garcia[1] · Mirta Fascio[1,2] · María Inés Errea[3] · Alain Dufresne[4] · Silvia Goyanes[5] · Norma D'Accorso[1,2]

Abstract Iron is an essential micronutrient for higher plants. Although abundant in most soils, Fe^{3+} is not available for plant uptake, because of its poor solubility. Ferrous sulfate is a fertilizer used for crops but, Fe^{2+} is readily oxidized to the plant-unavailable ferric form. It is therefore important to provide Fe^{2+} to plants, minimizing the loss of this nutrient by oxidation in Fe^{3+}. This paper reports the development of a composite material consisting of a matrix (PLARAM), obtained by the chemical modification of poly(lactic acid), capable of retaining ferrous carbonate (siderite) within PLARAM (PLARAMFe). From the matrix, Fe^{2+} is released into the soil, enhancing its bioavailability. PLARAM and PLARAMFe films were obtained and their water wettability was studied. One side of the films was more hydrophilic than the other, turning this material attractive as a protective film when it is necessary to avoid loss of humidity.

✉ Norma D'Accorso
norma@qo.fcen.uba.ar

1 CONICET- Universidad de Buenos Aires, Centro de Investigaciones en Hidratos de Carbono (CIHIDECAR), Buenos Aires, Argentina

2 Departamento de Química Orgánica, Facultad de Ciencias Exactas y Naturales, Universidad de Buenos Aires, Buenos Aires, Argentina

3 Instituto Tecnológico de Buenos Aires, Avenida Eduardo Madero 399, C1106ACD, Ciudad Autónoma de Buenos Aires, Argentina

4 Université Grenoble Alpes, CNRS, Grenoble INP, LGP2, 38000 Grenoble, France

5 Departamento de Física, FCEyN, UBA and IFIBA, Conicet, Pabellón 1, Ciudad Universitaria, 1428 Buenos Aires, Argentina

Keywords Bilayer · Biodegradable · Nano biocomposite · Poly(lactic acid) · L-Rhamnose · Siderite

Introduction

The adverse effects of human activities on the natural ecosystem are obviously increasing. As a result, nowadays, the scientific community is focused on finding new environmentally safe materials. Among all biopolymers based on renewable feedstock, poly(lactic acid) (PLA) is one of the most promising. PLA is hydrophobic aliphatic polyester, primarily produced by industrial polycondensation of lactic acid and/or ring-opening polymerization of lactide [1]. In the aquatic environment, it hydrolyzes into non-toxic hydroxycarboxylic acid through ester bond cleavage and then it is metabolized into water and carbon dioxide through a citric acid cycle [2].

PLA is classified as safe by the United State Food and Drug Administration (FDA) and has been approved for application in tissue engineering, medical materials, drug carriers and food packaging [2]. Besides, it has the potential to be used as a substitute for some of the existing polyolefin polymers [3]. To improve the physical properties of PLA, the addition of nanoparticles was explored [4, 5].

On the other hand, there are many reports on polymeric matrix designed to provide protection of entrapped active components to control the release of the bioactive compounds over time [6]. Particularly, PLA micro and nanoparticles have been widely studied as delivery systems for systemic and topical applications.

Given the above discussion, this paper reports the development of a composite material consisting of a matrix (PLARAM), obtained by chemical modification of

poly(lactic acid), capable of retaining ferrous carbonate within PLARAM (PLARAMFe).

Indeed, iron is an essential micronutrient for higher plants. Although abundant in most soils, Fe^{3+} is not available for plant uptake, because of its poor solubility. Although some plants have developed adaptation mechanisms that mobilize iron at the root-soil interface, symptoms of chlorosis frequently occur specially on calcareous soils. Ferrous sulfate is a fertilizer used for crops, but Fe^{2+} is readily oxidized to the plant-unavailable ferric form. It is therefore important to provide Fe^{2+} to plants, minimizing the loss of this nutrient by oxidation in Fe^{3+}. From the matrix, the Fe^{2+} ions were released into the soil, enhancing its bioavailability.

PLARAM and PLARAMFe films were obtained and their morphological, structural, thermal and water wettability properties were studied. One side of the films was more hydrophilic than the other, turning this material attractive as a protective film when it is necessary to avoid loss of humidity.

Experimental

Materials

Poly(lactic acid) pellets were provided by Shenzhen Bright China Industrial Co., Ltd. (Wuhan, China) (L-LA 90%, 10% D-LA). The number average molar weight (Mn = 77,408 g mol^{-1}) was determined by size exclusion chromatography (SEC). The weight average molar weight (Mw) and the polydispersity index were also determined and values of 213,323 g mol^{-1} and 2.8, respectively, were obtained. Prior to use, PLA was purified by dissolving it in dichloromethane and precipitating in methanol. Reagents were used as purchased (Sigma-Aldrich Co) without further purification. Solvents were reagent grade and they were dried and distillated before use according to standard procedures. The soil used was taken from Escobar [Buenos Aires, Argentina, pH 7.2; $CaCO_3$ (0.5%)]. Illite was found as the predominant clay mineral of the soil.

Synthesis of Siderite Nanoparticles

Siderite nanoparticles ($FeCO_3$) were synthesized according to the protocol proposed elsewhere [7, 8], with some modifications but, in our case, stoichiometric amounts of ferrous sulfate and potassium carbonate at pH 7 were employed. Besides, in order to prevent oxidation of iron(II) to iron(III), the synthesis was carried out under nitrogen atmosphere.

Potassium carbonate solution (1.8 g in 10 mL of deionized water) was added dropwise to the ferrous sulfate solution (2.0 g in 12 mL of deionized water). After 10 min of reaction, samples were placed into test tubes, under argon, and centrifuged at 2000 rpm for 15 min. After that, the supernatant was separated and the solid washed by re-suspension in deionized water and centrifugation. The procedure was repeated twice. Finally, the solid was suspended in anhydrous dichloromethane under argon and kept at low temperature.

Synthesis of PLARAM

PLARAM was obtained using the same procedure described for the grafting of modified PLA onto starch nanocrystals [9]. After protecting the terminal hydroxyl group of PLA by benzoylation (PLABz), the carboxyl acid was activated by reaction with thionyl chloride and the acyl chloride derivative obtained was further esterified by reacting with L-rhamnitol (Fig. 1).

Preparation of PLARAM Films

PLARAM was dissolved in chloroform and the solution was poured into a petri dish. The film was dried under vacuum for 50 h: the first 24 h at room temperature, the next 24 h at 40 °C and the last 2 h at 60 °C.

Preparation of PLARAMFe Films

PLARAM was dissolved in chloroform. The siderite nanoparticles were suspended in anhydrous dichloromethane and

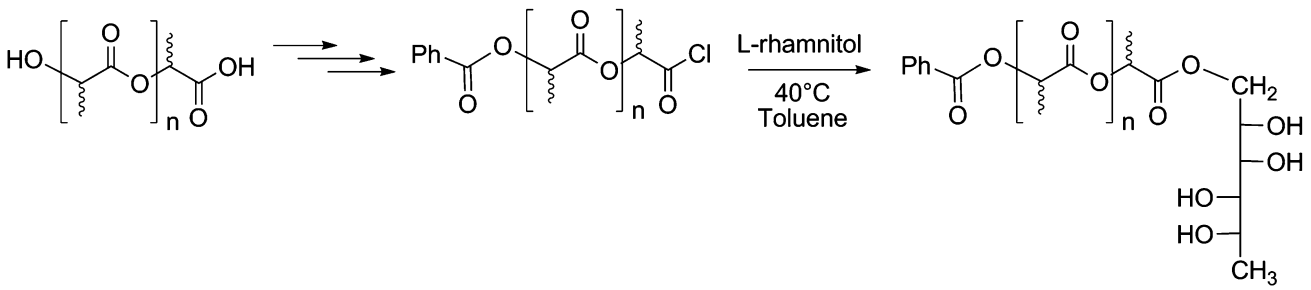

Fig. 1 Synthetic route to PLARAM

sonicated during 5 min. After that, the suspension of siderite was added to a chloroformic solution of PLARAM and left uncovered to allow the evaporation of the solvent. Then, the film was dried under vacuum for 50 h: the first 24 h at room temperature, the next 24 h at 40 °C and the last 2 h at 60 °C.

Field Emission Scanning Electron Microscopy (FE-SEM)

A SEM with field emission gun (FEG) Zeiss DSM982 GEMINI was used to examine the morphology of particles and films. Cryogenic fractured surfaces of films were examined. The samples were coated with a thin sputtered gold layer before analysis.

X-ray Photoelectron Spectroscopy XPS

X-ray spectroscopy was performed on a SPECS system equipped with a XR50 source and a hemispherical energy analyzer Phoibos MCD 100. The operating conditions are indicated on each spectrum. The energy scale was calibrated with a sample of Au-Cu: Au 4f7/2: 84.00 eV and Cu 2p3/2 932.66 eV. The effect of electrostatic charge is fixed in energy scale as internal reference using the C 1s peak at 285.0 eV. Settings Fe 2p peaks were performed using a Gaussian and Lorentzian product functions with the following restrictions: Spin–orbit splitting 13.6 eV; areas ratio of 2p3/2/2p1/2: 2/1 and Shirley line base type was used.

Elemental Analysis

Elemental analyses were performed on an Exeter Analytical CE-440 elemental analyzer. The result obtained for PLARAM was under the expected values.

Anal. calcd for $C_{8344}H_{11115}O_{5561}$: C 50.01, H 5.55; found: C 49.89, H 5.48.

Nuclear Magnetic Resonance (NMR)

^{1}H NMR spectra were recorded on a Bruker AC-200 spectrometer (200 MHz, $CDCl_3$). Chemical shifts (δ) are reported in parts per million (ppm) downfield from tetramethylsilane as internal standard.

Thermogravimetric Analysis (TGA)

Thermogravimetric analysis of the films was carried out using a Perkin-Elmer TGA-50H instrument under nitrogen atmosphere at 30 mL min^{-1} and at a heating rate of 5 °C min^{-1}. The temperature scan was run from room temperature to 400 °C.

Differential Scanning Calorimetry (DSC)

Analyses were performed with a DSC Q20 TA Instrument (New Castle, DE, USA) with a double cycle of heating from 25 to 200 °C at 10 °C min^{-1} separated by a single cooling cycle at 10 °C min^{-1} with isothermal step for 3 min 200 °C. The thermal history of the samples was erased by the preliminary heating cycle at 10 °C min^{-1}.

Contact Angle Measurements

The water wettability of the surface of PLA, PLARAM and PLARAM-Fe composite films was studied by static water contact angles (WCA) measurements, conducted with FTA 1000 Analyzer, at room temperature. The WCA analysis was assessed by measuring the angle of a 20 µL deionized water sessile drop on the polymeric surfaces. The average and the standard deviation of five independent measurements were taken.

Determination of Fe(III) by Thiocyanate Colorimetry

Concentration of Fe^{3+} in films samples was measured by thiocyanate colorimetry [10] using a UV–visible spectrophotometer Jenway 6705 at λ_{max} 479 nm.

Water Uptake Experiments

Water absorption studies were carried out by immersing the films (20 × 5 × 0.3 mm) in water at room temperature. The low thickness of the film allows the assumption of one-dimensional water diffusion. Samples were first dried at 100 °C under vacuum for one day. After weighing to determine the initial weight (Mo), they were placed in a container with 20 mL of distilled water. At specific time intervals (t), sample was weighted (M) until an equilibrium value was reached. Experiments were carried out in triplicate.

Results and Discussion

Characterization of Siderite Product

Field Emission Scanning Electron Microscopy (FE-SEM)

Size and morphology of siderite samples were determined by FE-SEM. Figure 2a shows the micrograph recorded at ×100 magnification where spherical domains with a size ranging from 600 nm to 1 µm can be observed. However, when the micrograph was recorded at ×200 magnification (Fig. 2b), it was possible to observe that these domains correspond to an organized nanoparticles surface, having diameter ranging from 40 to 60 nm. A similar observation

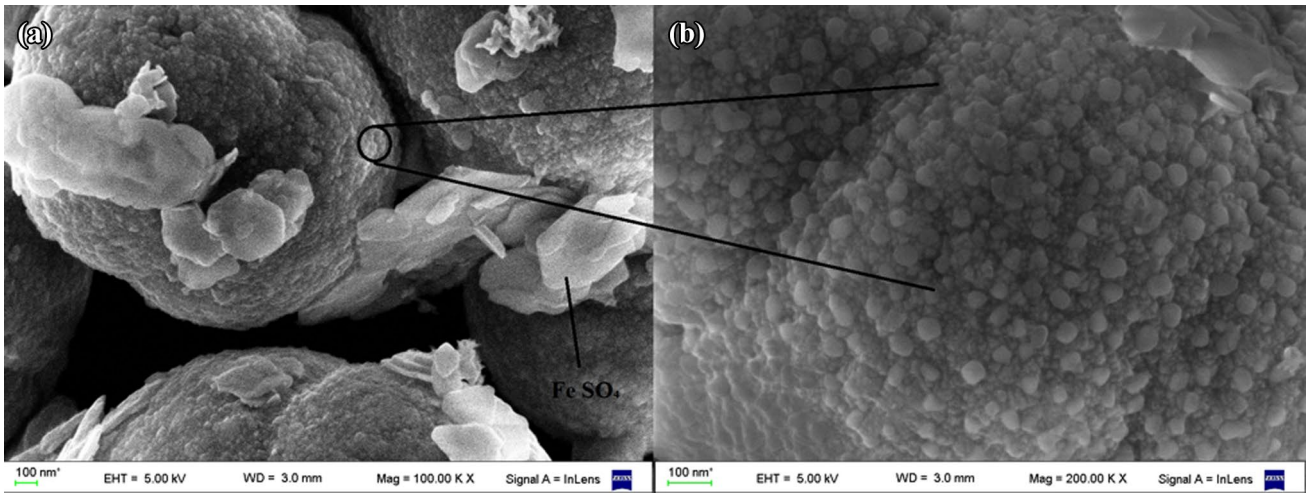

Fig. 2 FE-SEM micrographs of siderite $FeCO_3$ at 100 KX (**a**) and 200 KX (**b**)

was reported in other studies [11, 12]. According to Qu et al. [11], the formation of the microspheres was a consequence of a successive multistep growth process, which is driven by the intrinsic electric forces of siderite crystallites.

Besides, small amounts of hexagonal formations could also be observed in Fig. 2a. These formations, attributed to amorphous iron nanoplatelets, have a platelet morphology with an edge length of several ten of nanometers and a thickness of about 20–30 nm. The observation of these formations in the sample was attributed to the presence of unreacted ferrous sulfate. This is in agreement with the results previously reported by Guan et al. [12].

X-ray Photoelectron Spectroscopy (XPS)

Figure 3a shows the XPS spectrum for siderite, where it is possible to distinguish the photoemission peaks of Fe 2p, Fe 3P, Fe 3s O 1s and C 1s.

Figure 3b shows the spectrum for Fe 2p and its corresponding satellites. The spectra for Fe^{3+} and Fe^{2+} showed similar ranges of binding energy, differing in the peaks shape and in the intensity of their satellites. The XPS spectrum analysis allows us to infer that percentages of Fe^{2+} and Fe^{3+} in the sample were 50.5 and 49.5%, respectively. Since the XPS technique reflects changes in the surface, these results show that only half of the surface of siderite nanoparticles has been oxidized.

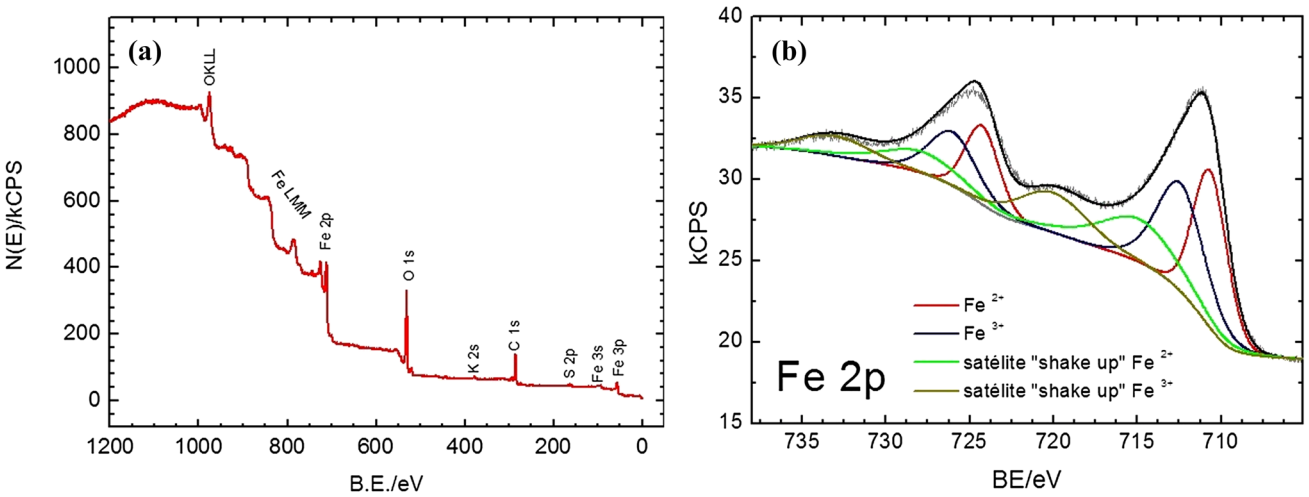

Fig. 3 **a** Global X-ray photoelectron spectrum for siderite ($FeCO_3$); **b** spectrum of the Fe 2p signal for siderite

Characterization of PLARAM

Nuclear Magnetic Resonance (NMR)

The transformation of PLA into PLARAM was confirmed by ^{1}H NMR spectroscopy (Fig. 4). Signals corresponding to aromatic protons of the benzoyl group linked to the terminal hydroxyl were observed between 7.2 and 8.1 ppm, while those corresponding to the carbohydrate linked to the carboxylic acid of the PLA were observed between 4.2 and 4.5 ppm. Besides, the main signals of the spectrum, observed at 1.6 and 5.2 ppm, where characteristic of PLA methyl and methine proton, respectively. The substitution degree was nearly 55% obtained from the relationship of the NMR area. We used the phenyl protons of benzoyl group (H-2 and H-5, 8.05 ppm) and methylene protons of carbohydrate moiety (4.40 ppm).

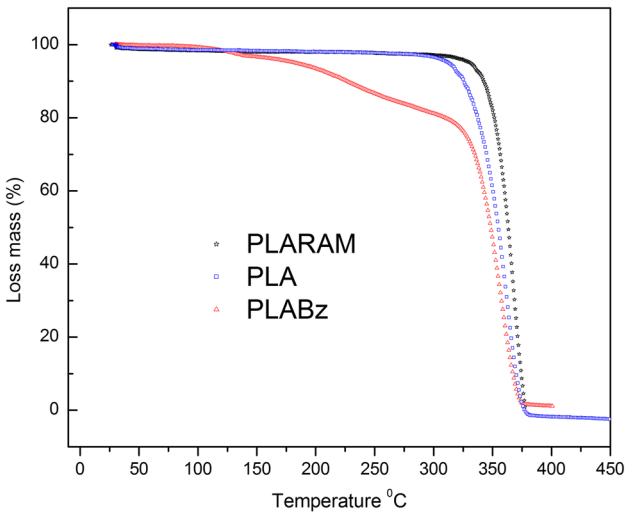

Fig. 5 TGA thermograms curves of PLARAM, PLA and PLABz

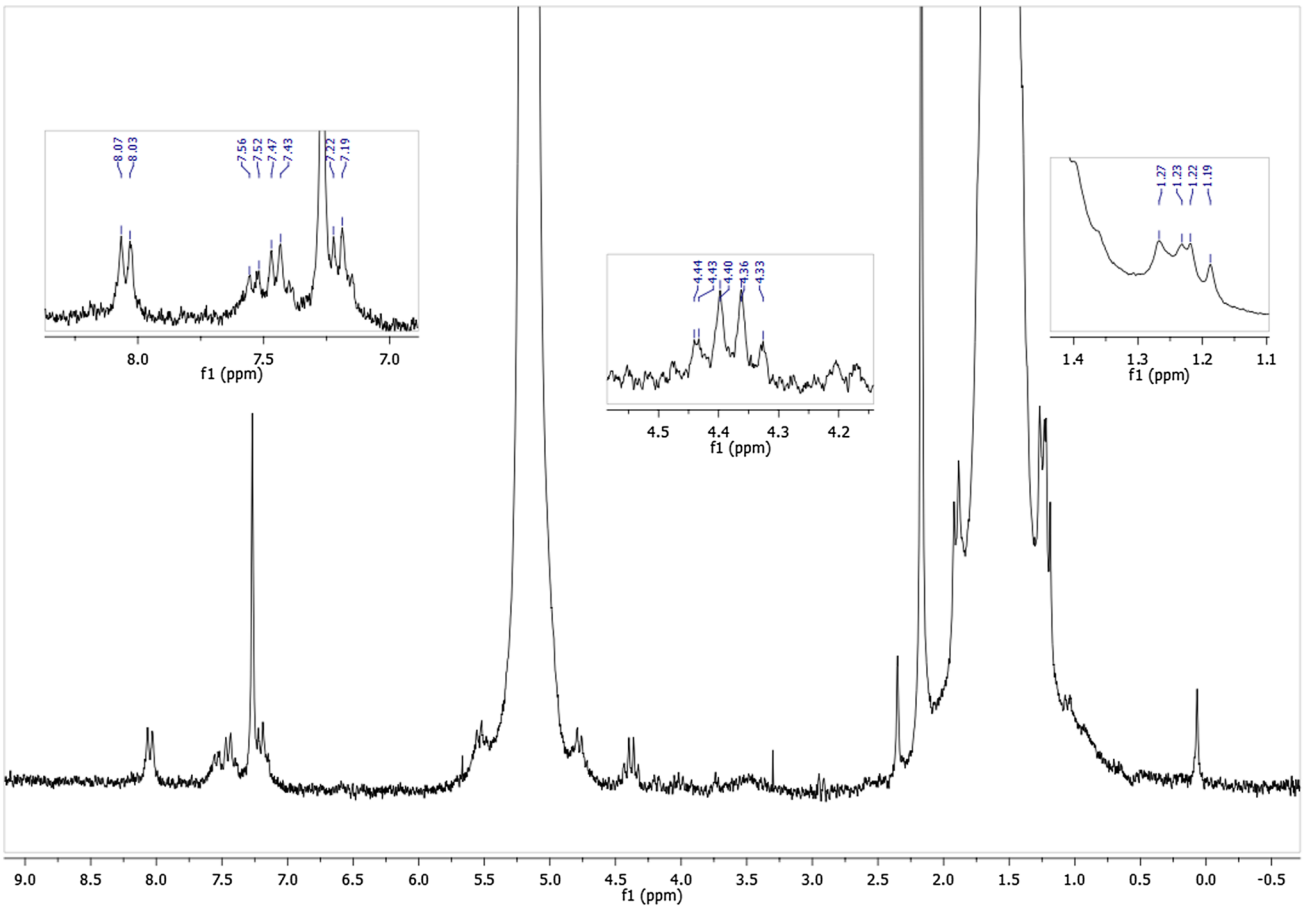

Fig. 4 ^{1}H NMR spectrum of PLARAM

Thermogravimetric Analysis (TGA)

Thermogravimetric analysis (TGA) was carried out to study the thermal stability of PLA, PLABz and PLARAM. Results are shown in Fig. 5.

The thermal degradation of PLA and PLARAM takes place in a single weight loss step. However, when thermal degradation of PLABz was carried out, two degradation steps were clearly observed which could be associated with two different degradation processes. The first process (between 219 and 275 °C) was assigned to the carboxyl group degradation. It is reasonable to not observe this step in the thermogram of PLA, because in this polymer the carboxyl group is stabilized by forming hydrogen bonds with the terminal hydroxyl group of another PLA chain. The second degradation process could be due to several decomposition reactions [13]. The thermal degradation of PLA is mainly associated with the hydrolysis of the ester groups and accelerated by the end groups (–COOH) [14].

On the other hand, the final temperature of degradation for PLARAM was about 377 °C indicating that, as expected, the transformation of PLA into PLARAM did not decrease the thermal stability of the polymer. Even more, a slight increase of the thermal stability was observed.

The increase in stability could be ascribed to the decreased amount of COOH groups which catalyze the decomposition of PLA.

The thermal stability of materials is always a desirable property given that, the greater thermal stability, the wider the range of possible applications.

Differential Scanning Calorimetry

Figure 6 shows the DSC thermograms (second heating scan) for PLA, PLABz and PLARAM.

The thermogram for PLA shows a heat flow change at 59 °C, corresponding to the glass transition temperature (Tg) of the polymer. Besides, a barely distinguishable melting endotherm could be observed at 150 °C. Tg of PLABz (32 °C) was lower than Tg of PLA. Besides, in the thermogram of PLABz, a crystallization exothermic peak can be observed between 80 and 110 °C, while the melting endotherm was observed as a double peak between 119 and 150 °C. Probably, the changes in the arrangement of the chains due to the incorporation of benzoyl groups increase the local free volume allowing the crystallization of the product.

On the other hand, for PLARAM, just a slight decrease of the Tg with respect to PLA was observed. Besides, in the case of PLARAM, the exothermic peak corresponding to crystallization was not observed, probably due to a depletion of the mobility of the chains of the PLARAM as a consequence of the hydrogen bonding established by the grafted rhamnose. However, as in the case of the PLA, a small melting peak can be observed at 153 °C.

Contact Angle Measurements

Contact angle measurement is one of the common ways to measure the wettability of the surface or a material. In this case, the contact angle was measured on both sides of PLA and PLARAM films, in order to confirm whether the condensation of PLA with an alditol could change the hydrophobicity of the material.

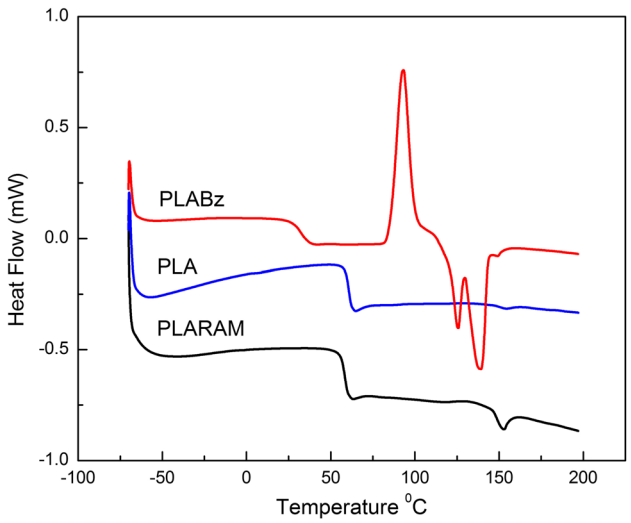

Fig. 6 DSC thermograms for PLARAM, PLABz and PLA

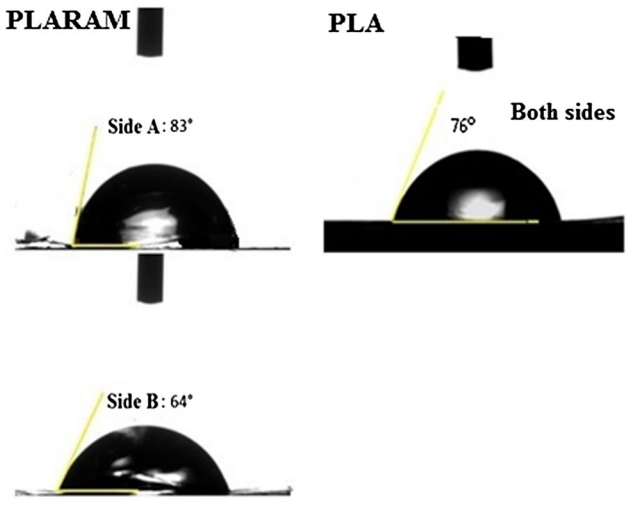

Fig. 7 Contact angle formed by a drop of water deposited on both sides for PLARAM and PLA films

Figure 7 shows the results. In the case of the PLA film, the same WCA was measured on both sides of the film (76° ± 1°). On the contrary, side A of the PLARAM film exhibited a contact angle higher (83° ± 1°) than for side B (64° ± 1°). It should be noted that the side A of the film was the one that was in contact with the petri dish.

This result suggests that side B of the film is more hydrophilic than side A. This was in agreement with a higher skin adherence for side B.

This is probably due to the fact that, when the film is forming, polar chains of rhamnitol are preferably oriented toward one side of the film (side B).

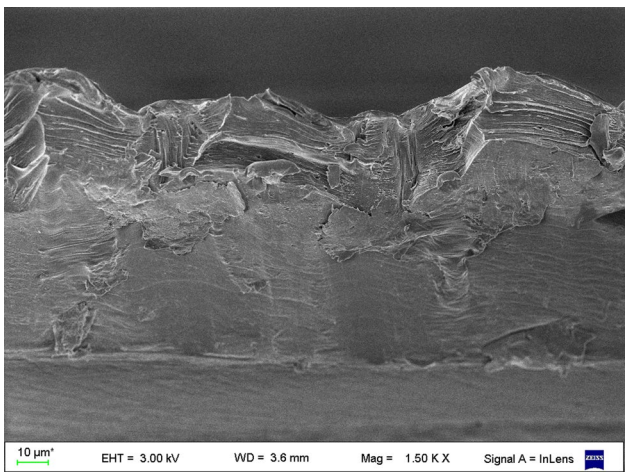

Fig. 8 FE-SEM micrograph of the cryo-fractured surface for PLARAM film

Morphological Characterization by SEM

The FE-SEM image of the cryo-fractured surface for PLARAM is shown in Fig. 8. Two layers morphology can be observed.

The upper region shows a superimposed lamellar sheets structure, whereas for the lower layer, the surface was smoother and more homogeneous. This type of morphology is repeated throughout all the fracture. This result is in concordance with the contact angle data, reinforcing the hypothesis that rhamnitol chains are ordered towards one of the sides of the film, leaving hydrophobic chains of PLA exposed to the other side (smoothest region of the micrograph).

Characterization of PLARAMFe

Morphological Characterization by FE-SEM

Figure 9 shows the micrographs of the cryo-fractured surface for PLARAMFe film.

As shown in Fig. 9a the morphology of the film changes dramatically with the addition of siderite nanoparticles. In this case, a patron veins effect is observed (top of the photo) as expected for composites generated by well-dispersed nanoparticles [15–17]. It would be expected that polar siderite nanoparticles were located in the rhaminol-rich area of the film, generating the discontinuity that can see in the image. In this respect, the hydrophobic film side area should correspond to the soft and smooth region (bottom of the photo).

Magnification of the micrograph of PLARAMFe (Fig. 9b) shows that, as was discussed above, particles of siderite are mainly located in the region in which the patron vein it is observed.

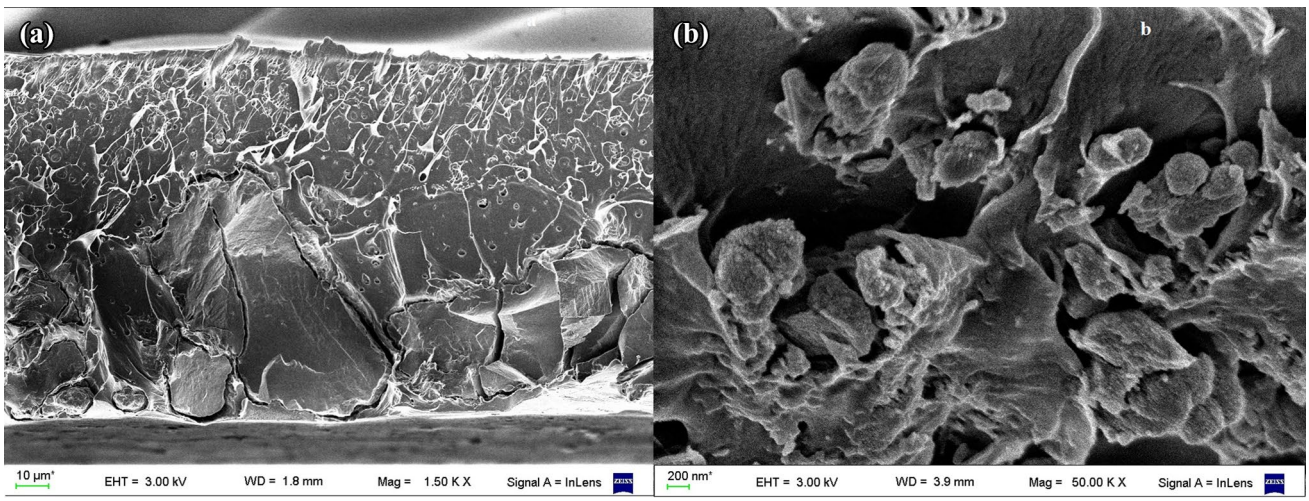

Fig. 9 FE-SEM micrographs of the surface for PLARAMFe at 1.50 KX (**a**) and at 50 KX (**b**)

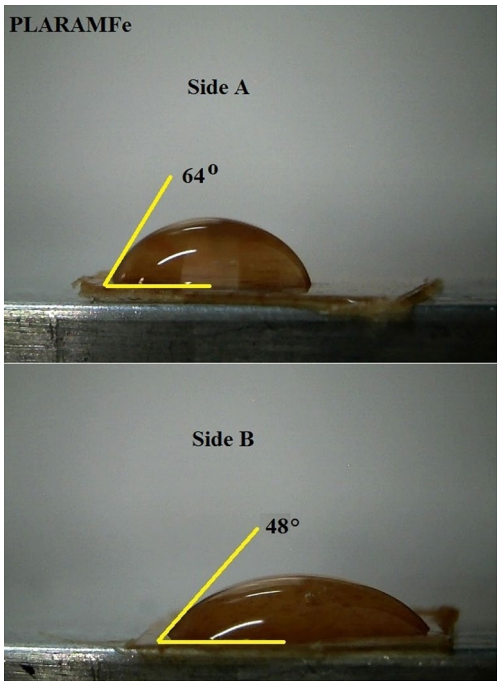

Fig. 10 Contact angle formed by a drop of water deposited on the both sides for PLARAMFe film

Contact Angle Measurements

Side A of the PLARAMFe film exhibits a WCA of 64° ± 1°, higher than that observed for side B (48° ± 1)° (Fig. 10).

These results show that, when adding siderite nanoparticles into the PLARAM film, the value of the contact angle changed for both sides of the film.

The increase of the hydrophilicity of B side is probably due to the pattern of veins caused by the addition of the siderite nanoparticles (Fig. 9), which improves the diffusion pathways of water molecules. The loss of hydrophobicity for the other side (side A), is probably because this area turns more brittle and cracked with the addition of iron (bottom of Fig. 9a) promoting the diffusion of water.

Water Uptake

When polymers are incorporated into soil, the stored water and fertilizer (siderite in this case) are gradually released to the soil. Thus, plant growth could be improved, and/or water supply conserved. It has been reported that increased water retention capacity attributed to polymer addition significantly reduced irrigation frequency and the total amount of irrigation water required [18].

Considering the relevance of the capacity of water retention of the material for its application in the field of agriculture, water uptake experiments were carried out.

Films were weighed at constant intervals of time until an equilibrium value was reached. At this moment, water absorption reached 5.0 and 13.7 wt% for PLARAM and PLARAMFe, respectively. Water absorption by the film was rapid at shorter times (< 24 h). After that, the rate of weight gain began to decline reaching a plateau after 15 days.

Release of Iron from PLARAMFe

The PLARAM film was loaded with 20 wt% of siderite nanoparticles, as described in the Experimental Section. The PLARAMFe film was buried for 15 days into the soil. After that time, a piece of the film was unearthed and its iron content was measured, finding that just 1.13% of the initial mass of iron was retained in the film. The procedure was repeated every 48 h for 10 days. The iron content of the last piece of film analyzed was 0.22%. This means that the release of iron from the film to the ground was almost quantitative. Besides, it was observed that the film began to degrade, since only 73% of the initial mass was recovered.

Conclusions

Chemical modifications of PLA allowed obtaining a new material (PLARAM), from which films were successfully obtained. In these films, Fe^{2+} ions could be incorporated (PLARAMFe), and the PLARAM matrix minimized the oxidation of Fe^{2+} to Fe^{3+}. In addition, the release of iron to the ground on which the films were buried was also verified. Besides, studies of water wettability of PLARAM and PLARAMFe films were carried out. One of the sides was more hydrophilic than the other, turning this material attractive as a protective film when it is necessary to avoid loss of humidity. Moreover, the degradation of the film that was observed in the tests performed, made even more attractive PLARAMFe to be used in the agriculture sector for prevention of iron chlorosis.

Acknowledgements The authors thank the financial support of UBACyT (No. 20020130100495BA and 20020130100021BA), ANPCyT (PICT- 2012-0717 and PICT-2012-1093), and CONICET (PIP 2013–2015, 11220120100508CO and 11220110100370CO).

References

1. Castro-Aguirre E, Iñiguez-Franco F, Samsudin H, Fang X, Auras R (2016) Poly(lactic acid)—mass production, processing, industrial applications, and end of life. Adv Drug Deliv Rev 107:333–366
2. Jamshidian M, Tehrany EA, Imran M, Jacquot M, Desobry S (2010) Poly-lactic acid: production, applications, nanocomposites, and release studies. Compr Rev Food Sci F 9(5):552–571

3. Sin LT, Rahmat AR, Rahman WAWA (2013) 1—overview of poly(lactic acid). In: Polylactic acid. William Andrew Publishing, Oxford, pp 1–70
4. Sinha Ray S, Okamoto M (2003) Polymer/layered silicate nanocomposites: a review from preparation to processing. Progr Polym Sci 28(11):1539–1641
5. Pluta M, Galeski A, Alexandre M, Paul MA, Dubois P (2002) Polylactide/montmorillonite nanocomposites and microcomposites prepared by melt blending: structure and some physical properties. J Appl Polym Sci 86(6):1497–1506
6. Sabliov C, Chen H, Yada R (2015) Nanotechnology and functional foods: effective delivery of bioactive ingredients. Wiley, Chichester
7. Helfferich FG (1962) Ion exchange. McGraw-Hill, New York
8. Del Campilllo Garcia MC, Sanchez Alcala I, Barron de la Torre V, Torrent Castelet J, Delgado Garcia A, Method for preventing and correcting iron chlorosis in plants. Patent WO2010076353: 2010
9. Garcia N, Lamanna M, D'Accorso N, Dufresne A, Aranguren M, Goyanes S (2012) Biodegradable materials from grafting of modified PLA onto starch nanocrystals. Polym Degrad Stab 97:2021–2026
10. Liu X, Wang H, Su C, Zhang P, Bai J (2010)) Controlled fabrication and characterization of microspherical $FeCO_3$ and α-Fe_2O_3. J Colloid Interface Sci 351(2):427–432
11. Qu X-F Y, Qi-Zhi Zhou, Gen-Tao (2011) Synthesis of siderite microspheres and their transformation to magnetite microspheres. Eur J Mineral 11(23):759–770
12. Guan J, Yan G, Wang W, Liu J (2012) External field-assisted solution synthesis and selectively catalytic properties of amorphous iron nanoplatelets. J Mater Chem 22(9):3909–3915
13. Kopinke FD, Remmler M, Mackenzie K, Möder M, Wachsen O (1996) Thermal decomposition of biodegradable polyesters—II. Poly(lactic acid). Polym Degrad Stab 53(3):329–342
14. Piemonte V, Gironi F (2013) Kinetics of hydrolytic degradation of PLA. J Polym Environ 21(2):313–318
15. García NL, Ribba L, Dufresne A, Aranguren MI, Goyanes S (2009) Physico-mechanical properties of biodegradable starch nanocomposites. Macromol Mater Eng294(3):169–177
16. Lamanna M, Morales NJ, García NL, Goyanes S (2013) Development and characterization of starch nanoparticles by gamma radiation: potential application as starch matrix filler. Carbohydr Polym 97(1):90–97
17. Zilli D, Chiliotte C, Escobar MM, Bekeris V, Rubiolo GR, Cukierman AL, Goyanes S (2005) Magnetic properties of multi-walled carbon nanotube–epoxy composites. Polym 46(16):6090–6095
18. Flannery RL, Busscher WJ (1982) Use of a synthetic polymer in potting soils to improve water holding capacity. Commun Soil Sci Plant Anal 13(2):103–111